Tirzepatide restricts obesity-related tumor growth by reversing metabolic dysregulation and rescuing CD8+ T cell function

Elaine M. Glenny[1], Michael F. Coleman[1], Genevieve T. Clutton[2], Brian P. Riesenberg[2], Alyssa N. Ho[1], Tori L. McFarlane[1], Violet A. Kiesel[1], Amanda L. Kucinskas[3], Emma G. Bailey[4], Katherine E. Sanchez[4], Jibin Zeng[5], Ye Wang[5], Hannah M. Malian[1], Claire E. Gates[1], Fangxin Chen[1], Ruihan Xu[1], C. Alex Holt[1], Evan M. Paules[1,7], Erin D. Giles[3,4,6], Jessica E. Thaxton[2,8,9*], Michael Pollak[5*], Stephen D. Hursting[1,7,8*]

1. Department of Nutrition, University of North Carolina at Chapel Hill, Chapel Hill, NC, USA
2. Immunotherapy Program, Lineberger Comprehensive Cancer Center, University of North Carolina at Chapel Hill, Chapel Hill, NC, USA
3. Department of Molecular & Integrative Physiology, University of Michigan Medical School, Ann Arbor, MI, USA
4. School of Kinesiology, University of Michigan, Ann Arbor, MI, USA
5. Departments of Oncology and Medicine, McGill University and Segal Cancer Centre, Jewish General Hospital, Montreal, QC, Canada
6. Rogel Cancer Center, University of Michigan, Ann Arbor, MI, USA
7. Nutrition Research Institute, University of North Carolina at Chapel Hill, Kannapolis, NC, USA
8. Lineberger Comprehensive Cancer Center, University of North Carolina at Chapel Hill, Chapel Hill, NC, USA
9. Department of Cell Biology & Physiology, University of North Carolina at Chapel Hill, Chapel Hill, USA

Key words: Obesity-associated cancer, tirzepatide, tumor-infiltrating lymphocytes (TILs), GLP-1 receptor (GLP1R), glucose-dependent insulinotropic polypeptide receptor (GIPR)

Funding: Financial support for this work was provided by the Breast Cancer Research Foundation (BCRF-23-073) and the UNC Triple Negative Breast Cancer Center to SDH, a Program Project grant from the Terry Fox New Frontiers to MP, and Ideas to Implementation Spark Award from RiseUp for Breast Cancer (Quantum Leap Healthcare Collaborative) to EDG.

Conflicts of interest: Evan M. Paules is a Balchem postdoctoral fellow. Balchem had no role in the study design, data collection, analysis, or preparation of the manuscript. The other authors declare no competing interests.

***Co-corresponding authors**

Stephen D. Hursting, PhD, MPH: hursting@email.unc.edu

Michael Pollak, MD: michael.pollak@mcgill.ca

Jessica E. Thaxton, PhD, MsCR: jess_thaxton@med.unc.edu

Abstract

Obesity, an established risk and progression factor for at least 13 cancer types, is highly prevalent globally, and effective strategies to mitigate the burden of obesity-related cancer are urgently needed. We investigated whether tirzepatide, a widely used incretin-mimetic drug that induces substantial weight loss, offers anticancer benefits. Across 3 tumor models, we demonstrate that chronic tirzepatide treatment reverses diet-induced increases in body weight and fat mass, systemic metabolic perturbations, and tumor growth. We also showed that the anticancer activity of tirzepatide does not involve direct effects on the neoplastic cells used, which lack incretin receptor expression. The anticancer actions of tirzepatide require the reversal of both the metabolic dysregulation and hyporesponsiveness of CD8+ tumor infiltrating lymphocytes evident in obesity. Our findings establish tirzepatide as a promising compound for intercepting obesity-related cancers.

Introduction

The global epidemic of obesity[1], which is a leading risk and progression factor for many common cancers[2], motivates the development of effective strategies to mitigate this dual public health crisis. Obesity drives multiple metabolic alterations, including hyperglycemia, hyperleptinemia, hyperinsulinemia, as well as low-grade chronic inflammation[3]. These perturbations foster an environment in which cancer cells receive mitogenic signals that not only accelerate proliferation, but also lead to increased uptake and utilization of macronutrients to the detriment of competing intratumoral immune cells[4-6]. Obesity further impairs antitumor immunity by engendering an immunosuppressive environment that protects tumor cells from the cytotoxic effects of CD8+ tumor infiltrating lymphocytes (TILs)[6-9].

Bariatric surgery is currently the most effective long-term weight loss strategy in patients with severe obesity, achieving >25% average total weight loss at 5 years accompanied by metabolic and immune reprogramming and a sustained 30-50% risk reduction in cancers associated with obesity[10,11]. However, bariatric surgery is expensive and only 1% of qualifying individuals in the United States undergo the procedure[12]. Lifestyle modifications through diet and/or exercise are generally accessible but typically result in only modest short-term weight loss that is challenging for most people to sustain[13,14]. Incretin-based pharmacotherapies, including semaglutide a glucagon-like peptide (GLP)-1 receptor agonist (GLP1RA) and tirzepatide a dual GLP-1 and glucose-dependent insulinotropic polypeptide (GIP) receptor agonist, are increasingly prescribed for the management of obesity and/or type 2 diabetes[15]. These drugs cause weight loss largely by acting in the central nervous system to suppress appetite and reduce food intake[16]. Tirzepatide, a highly effective weight loss drug approved by the US Food and Drug Administration in 2022, achieves an average sustained weight loss of 22.5% among adults with

83 obesity[17,18], reduces the risk of several chronic diseases, including type 2 diabetes[19] and
84 cardiovascular disease[20], and is safe and well tolerated over >3 years[21]. Incretin-mimetic agents
85 offer a promising, yet understudied, interception strategy for obesity-related cancers.

86 A study of patients with type 2 diabetes followed for 15 years showed that GLP1RA use,
87 relative to insulin use, was associated with lower risk of 10 of 13 obesity-related cancers,
88 particularly endometrial cancer in women and colon cancer in men[22]. In other studies of patient
89 cohorts with type 2 diabetes, associations of GLP1RA use and cancer risk were mixed[23-28]. These
90 retrospective pharmacoepidemiologic studies must be interpreted with caution due to lack of
91 randomization, particularly in the absence of supporting laboratory data and understanding of
92 underlying mechanisms. Early laboratory studies of first-generation GLP1RAs and cancer
93 progression showed inconsistent results[29], while studies of tirzepatide are sparse and have not
94 elucidated the underlying biology[30,31]. In experimental systems using next-generation incretin
95 mimetics, the extent of protection against obesity-driven tumor growth follows the extent of
96 weight loss achieved[32]. Herein, using multiple obesity-responsive syngeneic mouse transplant
97 models of cancer, we interrogated the effects of tirzepatide on systemic metabolism, antitumor
98 immunity, and tumor progression.

99

100 **Results**

101 ***Tirzepatide-associated weight loss in obese mice limits tumor growth and reverses metabolic***
102 ***perturbations***

103 We first determined if chronic administration of tirzepatide reduces obesity-driven tumor
104 growth in the immunogenic MC38 cancer model[6]. Diet-induced obese (DIO) mice received
105 subcutaneous injections of either tirzepatide (to promote weight loss) or vehicle (to maintain
106 obesity) for 3 weeks and were then transplanted with MC38 cancer cells (**Figure 1A**). Control

107 diet-fed mice were injected with vehicle and served as never-obese controls. A dose-finding
108 study in DIO mice was initially conducted to establish a tirzepatide regimen that achieves the
109 ~22% weight loss observed in human studies[17,18,21]. Weight loss was assessed over a range of
110 doses (1-30 nmol/kg) at different frequencies of administration (daily, every other day [q.o.d.],
111 and three times per week) for a 4-week duration (**Supplementary Figure 1**). Based on these
112 results, tirzepatide was administered in the current study q.o.d. using a progressive dose
113 escalation strategy (3-10 nmol/kg), with ~25% weight loss achieved by day 21 and maintained
114 (**Figure 1B**). As previously reported, the weight loss coincided with decreased caloric intake in
115 the setting of unrestricted food availability, with the largest reductions in food intake occurring
116 during the initial 4 weeks of tirzepatide treatment (**Figure 1B-C**)[33,34].
117 Along with inducing weight loss, chronic tirzepatide administration to DIO mice
118 significantly restricted tumor growth (**Figure 1D**) coincident with an improved metabolic profile
119 prior to cancer cell allograft. Specifically, tirzepatide drove substantial loss of total body mass,
120 with 78% of the weight loss attributed to fat mass, and reduction in fasting blood glucose levels
121 (**Figure 1E-H**). Several DIO-induced systemic metabolic perturbations were also reversed by
122 tirzepatide to resemble phenotypically never-obese controls, particularly i) leptin, which
123 decreased >9-fold; ii) insulin, which decreased 2-fold; and iii) adiponectin/leptin ratio, which
124 increased >9-fold (**Figure 1I-N**). Thus, tirzepatide reduces obesity and markedly improves the
125 metabolic milieu of DIO mice in association with reversal of obesity-driven MC38 tumor
126 growth.
127 To establish generalizability across sex and tumor type, we evaluated additional models.
128 Obese female mice were treated with similarly escalating doses of tirzepatide (3-30 nmol/kg) or
129 30% chronic calorie restriction, a gold-standard murine intervention to limit metabolic disease

130 and tumor growth. Tirzepatide and CCR both corrected metabolic abnormalities of obese mice,
131 reducing body weight and fat mass (**Supplementary Figure 2A-C**) and normalized the levels of
132 metabolic hormones and glucose in circulation (**Table S1**), with more substantial metabolic
133 effects elicited by CCR than by tirzepatide. Obesity-driven growth of E0771 tumors was blunted
134 by both tirzepatide and CCR (**Supplementary Figure 2D**). Similarly, tirzepatide treatment,
135 relative to vehicle treatment, in obese mice, resulted in a 40% reduction in transplanted ER+
136 Py230 tumor volume (**Supplementary Figure 2E**). Finally, terminal body weight was
137 significantly associated with tumor burden in both breast cancer models (**Supplementary Figure**
138 **2F-G**). Thus, the mitigation of obesity-driven tumor growth was consistent across multiple tumor
139 models and both sexes.
140
141 ***Tirzepatide efficacy is independent of direct GLP1R or GIPR engagement on MC38 tumor***
142 ***cells***
143 To address the mechanism underlying the antitumor activity of tirzepatide, we
144 investigated the possibility that the drug directly engages with GLP1R or GIPR on MC38 cancer
145 cells. Immunohistochemical analysis revealed that GLP1R protein (**Figure 1O**) was not
146 expressed in MC38 tumors (no validated antibody currently exists for murine GIPR[35]), consistent
147 with our analysis of the Cancer Cell Line Encyclopedia database[36] showing 0/80 human
148 colorectal cancer cell lines and 2/66 human breast cancer cell lines (and only 22/1437 of all
149 human cancer cell lines) express *GLP1R* at appreciable levels[37] (**Figure 1P)**. While 21/80 (25%)
150 human colorectal cancer cell lines and 21/66 human breast cancer cell lines (and 399/1437 of
151 total cancer cell lines) express low but discernible *GIPR* (**Figure 1Q)**, this is likely trivial in
152 murine models where GIPR is only engaged at high concentrations of tirzepatide (>30

153 nmol/kg)[38]. In addition, MC38 and E0771 cell viability in vitro was unaffected by exposure to
154 tirzepatide across a 1–500 nM dose range (**Figure 1R**). Accordingly, we dismissed direct effects
155 of tirzepatide on cancer cells as an explanation for the observed inhibition of allograft growth.
156

157 ***CD8+ TILs restrain tumor growth in tirzepatide-treated DIO mice***

158 We used bulk RNAseq of MC38, E0771, and Py230 tumors to reveal pathways and
159 processes altered by obesity (relative to control) that were normalized with chronic
160 administration of tirzepatide. Notably, features of antitumor immunity were consistently
161 suppressed by obesity but rescued with tirzepatide (**Supplementary Figure 2H**).

162 Obesity promotes an immunosuppressive tumor microenvironment that profoundly
163 impairs the ability of CD8+ TILs to effectively respond to and kill cancer cells[6-8]. We
164 hypothesized that tirzepatide-induced weight loss and reversal of obesity-associated metabolic
165 derangements would ameliorate the obesity-driven CD8+ TIL dysfunction that leads to a deficit
166 in antitumor immunity and increased tumor growth. To further investigate this hypothesis, we
167 relied on the MC38 tumor model as it is well characterized as both obesity-responsive and
168 immunogenic. Mice that received 21 days of vehicle or tirzepatide q.o.d., following 12 weeks of
169 control or DIO diet, were challenged with MC38 cancer cells, continued their assigned diet and
170 drug intervention, and were then euthanized after 14 days of tumor growth. We employed high-
171 dimensional flow cytometry analysis of tumoral and splenic CD8+ T cells to delineate obesity-
172 driven defects in antitumor immunity potentially rescued by tirzepatide. Uniform manifold
173 approximation and projection (UMAP) analysis of CD8+ TILs from tumors of vehicle-treated
174 control (never-obese) versus vehicle-treated DIO (always obese) mice identified 17 distinct
175 clusters (**Figure 2A-B**). CD8+ TILs from vehicle-treated never-obese mice were enriched in

176 clusters 1, 4, and 5 and were characterized by higher staining intensities for markers of activation
177 (CD44), effector function (GZMB), and exhaustion (CD39, PD-1, TIM-3, CTLA-4) (**Figure 2C-**
178 **D**). Conversely, CD8+ TILs from vehicle-treated DIO mice were enriched in clusters 15 and 17,
179 which had considerably lower staining intensity for markers of activation, effector function, and
180 exhaustion, and higher staining intensity for markers of non-activated and stem-like CD8+ TIL
181 states (TCF-1, CD62L, BCL-2) (**Figure 2C-D**).

182 We repeated the dimension reduction and clustering analysis, this time comparing CD8+
183 TILs from tirzepatide-treated DIO (formerly obese) mice versus vehicle-treated DIO (always
184 obese) mice. CD8+ TILs from vehicle-treated DIO mice were enriched in cluster 17 (non-
185 activated and stem-like TILs) and depleted in cluster 6 (activated and exhausted TILs) relative to
186 CD8+ TILs from tirzepatide-treated DIO mice (**Figure 2E-H**). Phenotypically, CD8+ TILs from
187 tirzepatide-treated DIO mice more closely resembled CD8+ TILs from vehicle-treated control
188 (never-obese) mice than from vehicle-treated DIO mice, as evidenced by median fluorescent
189 intensities (MFIs) of specific markers including CD62L, TCF-1, CD39, and PD-1 (**Figure 2I**).
190 The mitigating effect of tirzepatide on obesity-induced suppression of CD8+ T cells was limited
191 to TILs in the tumor microenvironment, as the immunophenotype of splenic CD8+ T cells from
192 vehicle- versus tirzepatide-treated DIO mice was similar (**Supplementary Figure 3**).
193 Collectively, these data suggest obesity engenders an immunosuppressive tumor environment
194 that enriches for a population of ineffective, non-activated CD8+ TILs, and that this
195 immunosuppressed phenotype is partially reversed with chronic tirzepatide treatment.

196 To assess if CD8+ TILs are essential for the anticancer benefit imparted by tirzepatide
197 treatment in the context of obesity, we depleted CD8α+ T cells in vehicle-treated mice on the
198 control diet, vehicle-treated DIO mice, and tirzepatide-treated DIO mice, all bearing MC38

199 tumors. CD8α+ T cells were systemically depleted beginning 2 days prior to MC38 transplant
200 (**Supplementary Figure 3B-D**). In mice treated with an isotype control IgG (non-neutralizing)
201 antibody, tirzepatide-treated DIO mice showed reduced MC38 tumor growth relative to vehicle-
202 treated DIO mice (**Figure 2J-K**). Depletion of systemic and tumoral CD8α+ cells did not further
203 accelerate tumor growth in obese mice whose TILs were already functionally compromised to
204 the extent that they were not effectively restraining neoplastic proliferation. However, CD8+ T
205 cell ablation did accelerate tumor growth in non-obese mice on the control diet and in
206 tirzepatide-treated DIO mice, revealing a clear impairment of antitumor immunity in response to
207 obesity which is reversible with tirzepatide (**Figure 2L-M**).
208
209 ***Direct receptor agonism on CD8+ TILs does not mediate the anticancer activity of tirzepatide***
210 GLP1R is reportedly expressed on a subset of activated T cells in various non-neoplastic
211 contexts, and GLP1R agonism alters T cell cytokine production[39-41]. However, as this
212 observation has yet to be tested in a cancer model, we first queried whether *GLP1R* and/or *GIPR*
213 were detectable in CD8+ T cells in the tumor microenvironment. Publicly available CD8+ TIL
214 single-cell sequencing data from B16 melanoma tumors (GSE245657) revealed that every CD8+
215 TIL cluster, with the notable exception of the CD8+ naïve T cell population, contained *GLP1R*
216 expressing cells (**Supplementary Figure 4A-C**)[8]. However, only 1.5% of the CD8+ TIL
217 population from either mice on the control diet or DIO mice expressed *GLP1R* (**Supplementary**
218 **Figure 4A-C**). *GIPR* was not detected in any CD8+ TIL population.
219 Since the single-cell RNA sequencing analysis showed that *GLP1R,* but not *GIPR*, was
220 detectable in a subset of CD8+ TILs, we next sought to determine whether direct *GLP1R*
221 agonism on CD8+ TILs contributes to the anticancer and immunomodulating effects of

222 tirzepatide observed herein. Congruent with published reports[39-41], further analysis of the single-
223 cell data (GSE245657) revealed pathways involved in T cell activation, differentiation,
224 chemotaxis, and interferon-mediated signaling were uniformly suppressed in activated *GLP1R*+
225 TILs relative to activated *GLP1R*- TILs, as determined by GSEA of gene ontology biological
226 process (GOBP) (**Supplementary Figure 4D**). Moreover, in vitro tirzepatide treatment modestly
227 suppressed the cytotoxic function of in vitro-activated CD8+ splenocytes from tumor-bearing
228 DIO mice, as indicated by reduced IFNγ and TNFα production (**Supplementary Figure 4E-G**).
229 Collectively, these data indicate that *GLP1R* expression on CD8+TILs cells is scant, *GIPR* is
230 undetectable, and agonism of GLP1R in CD8+ TILs is modestly immunosuppressive. Thus,
231 direct receptor agonism on CD8+ TILs is unlikely to mediate the antitumor effects of tirzepatide
232 in obese mice.
233
234 ***Tirzepatide fails to limit MC38 tumor growth or improve CD8+ T cell response in lean mice***
235 Since the anticancer effects of tirzepatide require CD8+ T cells but not direct receptor
236 engagement on either tumor or CD8+ T cells, we explored the possibility that reversing obesity-
237 associated metabolic dysfunction is key to the inhibitory effect of tirzepatide on obesity-
238 stimulated MC38 tumor growth. We transplanted MC38 cells into lean (never-obese) mice fed an
239 ad libitum control diet (10 kcal% fat) and then randomized the mice to receive vehicle or
240 tirzepatide injections q.o.d. for the next 20 days (**Figure 3A**). Tirzepatide did not affect tumor
241 growth in these lean, metabolically healthy mice despite achieving modest reductions in food
242 intake, body weight, blood glucose, and serum levels of insulin, IGF-1, and leptin (**Figure 3B-J**).
243 Importantly, in these lean mice, baseline hormone levels were lower, and the reductions were
244 smaller in magnitude, than those seen in DIO mice treated with tirzepatide (**Figure 1**). To

245 evaluate whether tirzepatide had an effect on remodeling CD8+ TIL populations in lean mice, we
246 performed high-dimensional flow cytometry on tumoral and splenic CD8+ T cells following 14
247 days of MC38 tumor growth. Unlike our observations in tirzepatide-treated DIO mice,
248 tirzepatide treatment in lean mice skewed CD8+ TILs towards a less differentiated phenotype, as
249 evidenced by increased CD62L and SlamF6 and reduced CD44, T-bet, TOX, and CD27
250 (**Figure 3K-L**). Thus, neither the tumor growth inhibitory effects nor the immune-enhancing
251 effects of tirzepatide observed in obese mice were evident in metabolically healthy lean mice.
252 This indicates that tirzepatide enhances anticancer immunity in obese mice indirectly, by
253 ameliorating endocrine or metabolic abnormalities associated with obesity. This is consistent
254 with prior evidence that obesity-related endocrine abnormalities such as hyperleptinemia
255 compromise anticancer immune function[42,43].
256

257 **Discussion**

258 We demonstrate that chronic tirzepatide treatment reverses obesity-associated increases
259 in body weight, fat mass, and systemic metabolic perturbations, and reduces tumor growth in
260 three murine cancer models. The antitumor effects of chronic tirzepatide treatment in obese
261 mice, on colon and breast cancer models are consistent with our findings in a murine model of
262 endometrial cancer[30], as well as a report by others on liver cancer[36], and are further supported by
263 reports that significant weight loss (at levels similar to those achieved with tirzepatide) in
264 response to chronic or intermittent calorie restriction or bariatric surgery have anticancer effects
265 in multiple obesity-related cancer models[44-46]. Moreover, emerging pharmacoepidemiologic
266 evidence suggests that use of GLP1RA for the management of type 2 diabetes may lead to

267 reduced risk of most obesity-related cancers[22]. Together, these findings suggest that use of
268 tirzepatide is a promising interception strategy for obesity-associated cancers.

269 A novel finding in the present study is that tirzepatide exerts its anticancer effects by
270 reversing CD8+ T cell-associated immunosuppression in the tumor microenvironment. We
271 demonstrate that tirzepatide restored expression of transcriptomic signatures of antitumor
272 immunity which were suppressed by obesity in multiple tumor models. In particular, a role for
273 CD8+ TIL function on limiting MC38 tumor growth in tirzepatide-treated obese mice is
274 established by the loss of tirzepatide's beneficial effects upon systemic CD8+ T cell depletion
275 with a neutralizing antibody. Obesity engenders an environment whereby CD8+ TILs are
276 ineffective and hyporesponsive, resulting in rapid acceleration of tumor growth[6-8]. Indeed,
277 obesity-driven defects in CD8+ TIL activation curtail the requirement for T cell extrinsic
278 immune evasion to the point where tumors transplanted from obese mice into
279 immunocompromised mice grow more slowly than those transplanted from never-obese control
280 mice[8]. We demonstrate that tirzepatide protects against CD8+ TIL inactivity by reversing
281 phenotypic markers of obesity-associated immunosuppression (decreased CD62L, TCF1;
282 increased CD39, PD-1 relative to tumors from vehicle-treated DIO mice).

283 Direct effects of tirzepatide on MC38 colonic adenocarcinoma cells via agonism of
284 incretin receptors to promote cytotoxicity are unlikely given the lack of expression of both
285 GLP1R and GIPR on these cells, and the lack of response of these cells to tirzepatide across a
286 wide dose range in vitro. However, direct effects of GLP1R agonism on CD8+TILs are
287 plausible, given reports of GLP1R upregulation in activated TILs[39-41] and our observation from
288 single-cell sequencing data that a subset of activated CD8+ TILs express *GLP1R*. Further
289 analysis of single-cell sequencing data indicated that *GLP1R*+ CD8+ TILs, relative to *GLP1R*-

290 TILs, displayed uniform suppression of pathways involved in T cell activation and
291 differentiation, chemotaxis, and interferon-mediated signaling, suggesting that direct effects of
292 tirzepatide on CD8+ TILs are unlikely to explain its anticancer benefits. We further showed that
293 agonism of GLP1R with tirzepatide in ex vivo splenocytes isolated from tumor-bearing DIO
294 mice modestly suppressed CD8+ T cell effector function. Others have also indicated that GLP1R
295 agonism on CD8+ T cells is immunosuppressive, as GLP1R on activated T cells acts as a
296 negative costimulatory molecule akin to PD-1[39]. Congruently, GLP1R agonists exendin-4 and
297 liraglutide suppress CD8+ T cell proliferation and cytokine production (consistent with our in
298 vitro findings) to curb inflammation and ameliorate systemic and localized inflammatory
299 conditions[39-41,47,48]. We thus conclude that direct engagement of the intended targets of
300 tirzepatide, the GLP-1 and GIP receptors, on CD8+ TILs is not substantially involved in the
301 antitumor effects of tirzepatide in obese mice.
302 There is a dearth of actionable targets for restoring CD8+ TIL functionality in the context
303 of obesity[6-8,43], and our finding that tirzepatide is able to do so, possibly via systemic metabolic
304 reprogramming, may inform future studies. For example, circulating leptin, which is increased
305 >9-fold in response to DIO but is largely normalized by tirzepatide treatment, is directly
306 proportional to fat mass, and frequently implicated in suppressing antitumor immunity[9,42]. Leptin
307 agonism of the leptin receptor (LEPR) on CD8+ T cells suppresses CD8+ TIL effector function,
308 while CD8+ T cells lacking LEPR limit tumor growth in Rag2$^{-/-}$ mice to a greater extent than
309 LEPR-expressing T cells[9,42]. In addition, obesity-associated increases in leptin and other
310 metabolic and inflammatory signals impairs antigen presentation by tumor-associated
311 macrophages, thus preventing the proper activation and clonal expansion of antigen-reactive
312 CD8+ TILs[43].

313 We found that tirzepatide was ineffective at suppressing tumor growth in lean mice,
314 suggesting resolution of underlying metabolic dysfunction (such as hyperleptinemia) is a
315 predominant means through which tirzepatide protects against obesity-driven tumor growth.
316 Consistent with this finding, Piening et al. recently demonstrated that weight loss through dietary
317 restriction enhanced antitumor immunity in a B16-F0 mouse melanoma model, but a suboptimal
318 semaglutide dosage that failed to resolve obesity-driven metabolic dysfunction did not[8].
319 We conclude that the health benefits of incretin-mimetic drugs such as tirzepatide in
320 individuals with obesity may include intercepting obesity-related cancers via improved antitumor
321 immunity. While we show that tirzepatide clearly reduces the growth rates of established cancers
322 in allograft models, additional laboratory studies are needed to further elucidate mechanism and
323 to clarify if tirzepatide influences early steps of carcinogenesis. Long-term randomized clinical
324 trials of incretin-mimetic drugs with cancer incidence or progression endpoints would be
325 logistically challenging but clinical intervention studies with tissue and circulating biomarker
326 endpoints are justified.

327 **Methods**

328 ***Mice***

329 All studies were approved by the Institutional Animal Care and Use Committee at the
330 University of North Carolina–Chapel Hill or the University of Michigan. C57BL/6J diet-induced
331 obese (DIO; stock #380050) and age-matched control male mice (stock #000664) were
332 purchased from the Jackson Laboratory at 10-16 weeks of age (Bar Harbor, ME). Female
333 C57BL/6NCrl mice were purchased at 10 weeks of age (Charles River, Wilmington, MA). Mice
334 were housed in a specific-pathogen-free facility with a 12 h light (7am-7pm)/12 h dark (7pm-
335 7am) cycle, and cages were changed weekly to refresh diet and ALPHA-dri™ bedding

336 (Shephard Specialty Papers, Watertown, TN). Obese mice and age-matched control mice used
337 for E0771 and MC38 tumor models were fed ad libitum a 60 kcal% fat diet (DIO; D12492
338 Research Diets, Inc, New Brunswick, NJ) or 10 kcal% fat diet (control; D12450J Research Diets,
339 Inc.), respectively. CCR was implemented by providing mice a daily aliquot of a high protein
340 diet (D15032801, Research Diets Inc.), to achieve a 30% reduction in caloric intake with
341 adequate micronutrient consumption relative to controls. Mice used for Py230 tumor model
342 underwent a modified diet-induced obesity program relying on a lower fat diet but housed in
343 thermoneutral conditions to reduce energy expenditure[49]. These mice were housed at 28°C–31°C
344 to limit adaptive thermogenesis and provided a 40 kcal% fat 39 kcal % sugar diet ad libitum
345 (D15031601; Research Diets, Inc.). Body composition was assessed by magnetic resonance
346 imaging (EchoMRI, Houston, TX). Mice were euthanized with CO_2 inhalation followed by
347 cervical dislocation or exsanguination while under isoflurane anesthesia.
348
349 ***Tirzepatide dosage***
350 After a minimum of 12 weeks on diet, DIO mice were randomized by body weight to
351 remain obese or lose weight via tirzepatide (LY3298176, Selleck Chemicals, Houston, TX) while
352 continuing the 60 kcal% fat diet. Mice were subcutaneously injected with either vehicle (5%
353 DMSO/95% 40 mM Tris pH 8.0) or tirzepatide (dose ranging from 1-30 nmol/kg in pilot dose-
354 finding study, 3-10 nmol/kg in tumor studies in male mice, 3-30 nmol/kg in female mice, and 3-
355 75 nmol/kg in female mice housed at thermoneutrality; frequency ranging from daily to q.o.d.)
356 for the remainder of each study. Injections occurred between 3:30-6:00 pm to proceed the onset
357 of the dark cycle.
358

359 ***Fasted blood glucose measurements***

360 Mice were fasted for 5 h. Blood was collected from the tail vein, and glucose
361 concentration was measured using a Contour Next EZ blood glucometer (Bayer, Jamestown,
362 NC). For intraperitoneal glucose tolerance tests, mice were injected with a bolus of 1.5 mg/kg D-
363 glucose, and blood was collected and read on a glucometer at 0, 15, 30, 60, 90, and 120 min.
364

365 ***Circulating hormone and cytokine concentrations***

366 Mice were fasted 4-5 h prior to collection of submandibular (prior to tumor injection) or
367 cardiac blood (at study termination). Blood samples clotted at RT for 30-60 min and were
368 centrifuged at 1000 x g for 15 min at 4 °C. Serum was aliquoted, flash frozen in liquid N_2, and
369 stored at -80 °C. Serum hormone concentrations were quantified using the Bio-Plex Pro Mouse
370 Diabetes 8-plex and Adiponectin assays (Bio-Rad Laboratories, Hercules, CA), and IGF-1 mouse
371 Luminex discovery assay (R&D Systems, Minneapolis, MN) using the Luminex platform. In the
372 study using only lean mice, a smaller marker panel was used that included mouse insulin (Crystal
373 Chem, Elk Grove Village, IL), mouse leptin (Crystal Chem), and total mouse IGF-1 (Ansh Labs,
374 Webster, TX), each measured by ELISA according to manufacturers' instructions.
375

376 ***Tumor cell transplantation***

377 MC38 (Kerafast, Boston, MA) and E0771 (CRL-3461, ATCC, Manassas, VA) cells were
378 maintained at 37 °C with 5% CO_2 in Dulbeco's Modified Eagle Medium containing 4.5 g/L
379 glucose (Gibco, Carlsbad, CA) and supplemented with 10 mM HEPES buffer (Gibco), 10% fetal
380 bovine serum (VWR International, Radnor, PA), 2 mM glutamine (Gibco), and 1% penicillin
381 streptomycin (Gibco). Py230 cells (provided by Nicholas Webster and Lesley Ellies, University

382 of California San Diego) were maintained in F12K Nutrient Mixture (Corning 10-025-CV)
383 supplemented with 5% Fetal Clone II (Cytiva SH30066.03), 50 µg/mL gentamycin (Sigma-
384 Aldrich G1397), 2.5 µg/mL amphotericin B (Sigma-Aldrich A2942), and 1 µL/mL MITO+
385 Serum Extender (Corning 355006) at 37 °C and 5% CO_2. Cells were routinely tested for the
386 presence of mycoplasma using the Universal Mycoplasma Detection Kit (ATCC). Mice were
387 subcutaneously injected with 2.5 x 10^5 MC38 cells into the right flank. Mammary cancer tumors
388 were achieved by orthotopically injecting 3.5 x 10^4 E0771 cells or 1 x 10^4 Py230 cells in 2
389 mg/mL Matrigel (Corning 356234) into the 4th mammary fat pad. Tumor growth was monitored
390 every 2-3 days using digital calipers. Tumor volume was calculated as D x d^2 x 0.5 where D is
391 the diameter of the longer dimension and d is the diameter perpendicular to D[50].
392
393 ***CD8+ cell depletion***
394 Mice were intraperitoneally injected with either 200 µg rat IgG2b isotype control
395 (#BE0090, clone LTF-2; Bio X Cell, Lebanon, NH) or 200 µg αCD8α (#BE0061, clone 2.43;
396 Bio X Cell). Relative to the day of MC38 tumor cell injections, isotype control and αCD8α
397 antibodies were injected on days -2, 0, 2, and every 4 days thereafter.
398
399 ***High-dimensional flow cytometry***
400 Tumors were dissociated using the Miltenyi Biotec (Bergisch Gladbach, Germany)
401 mouse tumor dissociation kit and gentleMACs dissociator according to manufacturer's
402 instructions but reducing enzyme R to 20% of suggested volume. Leukocytes were enriched
403 using Percoll density gradient centrifugation. Spleens were mechanically digested and filtered

404 through a 70 μm cell strainer, and red blood cells were lysed with ammonium-chloride-potassium
405 buffer (Gibco).
406 For T cell phenotyping, cells were stained in PBS for 30 min at 4 °C with Zombie NIR
407 viability dye (1:7000; Biolegend, San Diego, CA), CD45-BV510 (1:1000; BD Biosciences,
408 Franklin Lakes, NJ), CD8α-Spark NIR 685 (1:1000; Biolegend), CD4-APC Fire 810 (1:1000;
409 Biolegend), CD11b-Alexa Fluor 532 (1:5000; Invitrogen), TCRβ-BV570 (1:100; Biolegend),
410 CD44-Brilliant Violet 785 (1:400; Biolegend), CD62L-BV421 (1:400; BD Biosciences), PD-1-
411 BB700 (1:200; BD Biosciences), TIM-3-BV711 (1:200; Biolegend), LAG-3-APC-eFluor 780
412 (1:200; Invitrogen), SlamF6-APC (1:200; Invitrogen), CD39-Super Bright 436 (1:200;
413 Invitrogen), CX3CR1-PE-Fire 640 (1:200; Biolegend), CD69-PE-Cy5 (1:600; Biolegend),
414 GITR-BV650 (1:400; BD Biosciences), CD27-BV750 (1:200; BD Biosciences), and
415 CD16/CD32-purified FcR block (Invitrogen). Cells were washed and fixed overnight using the
416 Foxp3/Transcription Factor Fixation/Permeabilization Concentrate and Diluent kit (Invitrogen).
417 Cells were then washed and stained with T-bet-eFluor 450 (1:100; Invitrogen), CTLA-4-PE-
418 Dazzle 594 (1:400; Biolegend), Ki67-BV605 (1:400; Biolegend), TOX-PE (1:100; Miltenyi
419 Biotec), TCF-1-PE-Cy7 (1:100; Cell Signaling Technology, Danvers, MA), Granzyme B-Alexa
420 Fluor 700 (1:200; Biolegend), and BCL-2-Alexa Fluor 647 (1:400; Biolegend) for 3 h at RT.
421 For splenic and intratumoral CD8+ T cell depletion assessment, cells were incubated with
422 TruStain FcX (Biolegend) in PBS for 15 min at 4 °C. Cells were stained with LIVE/DEAD
423 fixable blue dead cell stain (1:1600; Invitrogen), CD45-BUV395 (1:300; BD Biosciences), CD4-
424 BUV805 (1:200; BD Biosciences), CD8α-Alexa Fluor 594 (1:200; Biolegend), and CD3-Alexa
425 Fluor 700 (1:200; Biolegend). To assess CD8+ T cell enrichment from splenocyte preparations,
426 cells were additionally stained with rat anti-mouse CD11c-BUV737 (1:100; BD Biosciences),

427 CD11b-PerCP-eFluor 710 (1:100; Invitrogen), and CD19-PerCP (1:75; Biolegend). Cells were
428 fixed using a cytofix/cytoperm fixation/permeabilization kit (BD Biosciences).
429 Events were collected on a Cytek Biosciences (Fremont, CA) Aurora or Northern Lights
430 full spectrum flow cytometer. Data were analyzed using FlowJo (v.10.8.1; Ashland, OR) and
431 OMIQ software (Dotmatics, Boston, MA).
432
433 ***CD8+ splenocyte in vitro activation and expansion***
434 CD8+ T cells were isolated from spleens from tumor-bearing obese mice by negative
435 magnetic selection (STEMCELL Technologies, Vancouver, Canada). Isolated cells were
436 activated with 5 μg/ml plate-bound αCD3, 2 μg/ml soluble αCD28 (eBioscience, San Diego,
437 CA), and 200 units/ml IL-2 (TECIN) and treated with 0-1000 nM tirzepatide for 3 days in RPMI
438 supplemented with 10% FBS, 300 mg/L L-glutamine, 100 units/mL penicillin, 100 μg/mL
439 streptomycin, 1mM sodium pyruvate, 100 μM NEAA, 1 mM HEPES, 55 μM β-mercaptoethanol,
440 and 0.2% plasmocin mycoplasma prophylactic. On day 3, media was replaced as at day 0, except
441 lacking αCD3 and αCD28. Cytokine production was assessed on day 5 following 5 hours of
442 restimulation with PMA/ionomycin [Cell Stimulation Cocktail (Thermo Fisher Scientific) at
443 1:500].
444
445 ***Cell viability assays***
446 5 x 10^2 MC38 or E0771 cells were seeded in complete media in a 96-well plate. Media
447 was replaced 4 h after seeding with complete media containing 0-500 nM tirzepatide. Media
448 (with or without tirzepatide) was replaced once after 44 h. 72 h after seeding, cells were
449 incubated in 3-(4,5-dimethylthiazol-2-yl)-2,5-diphenyltetrazolium bromide (MTT) reagent for 75

450 min. Formazan was solubilized in 100 µl DMSO, and the relative absorbance at 570 nm
451 subtracted from background absorbance at 690 nm was measured on a Cytation3 plate reader
452 (BioTek Instruments; Winooski, VT) to assess cell viability.
453
454 ***Immunohistochemistry***
455 Tissues were fixed in 10% neutral-buffered formalin for 24 h and stored in 70% ethanol
456 at RT. Paraffin-embedded tissue was baked overnight, deparaffinized, rehydrated, and underwent
457 heat-induced epitope retrieval using Borg Decloaker (Biocare Medical, Pacheco, CA) and a
458 decloaking chamber (120 °C for 30 sec followed by 90 °C for 10 sec). Slides were incubated in
459 3% hydrogen peroxide for 10 min at RT and then permeabilized and blocked in 5% normal goat
460 serum for 1 h at RT. Slides were incubated overnight at 4 °C with α-GLPR (1:500, rabbit,
461 ab218532; Abcam, Cambridge, United Kingdom). Slides were then sequentially incubated with
462 biotinylated α-rabbit IgG (1:500, goat, #111-065-144; Jackson ImmunoResearch Labs, West
463 Grove, PA) for 1 h at RT and an ABC Elite reaction kit (1:50, #PK-6100; Vector Laboratories,
464 Burlingame, CA). Positive signal was detected with diaminobenzidine (Thermo Fisher
465 Scientific), and slides were counterstained with hematoxylin.
466
467 ***Cancer Cell Line Encyclopedia gene expression analysis***
468 Human cancer cell line gene expression data was accessed from the Broad Institute's
469 Cancer Cell Line Encyclopedia through the Depmap portal[36]. "Batch corrected Expression Public
470 24Q2" was downloaded with metadata. A cancer cell line *GLP1R* or *GIPR* expression of
471 log2(TPM+1) >2 was deemed to be appreciable[37].
472

473 ***Bulk RNA sequencing***

474 RNA was isolated from whole tumors using the RNeasy micro kit (Qiagen), quantified
475 using a Qubit 2.0 fluorometer (Life Technologies, Carlsbad, CA), and assessed for integrity using
476 a TapeStation 4200 (Agilent Technologies, Santa Clara, CA). NEBNext Ultra II RNA libraries
477 were prepared (New England Biolabs, Ipswitch, MA) with an ERCC RNA spike-in (Thermo
478 Fisher Scientific) and sequenced using an Illumina HiSeq with a 2 x 150 bp paired-end
479 configuration targeting >25 million reads per sample. Adapters and low-quality reads were
480 removed with Trimmomatic[51]. Spliced Transcripts Alignment to a Reference (STAR) was used to
481 align reads to the GRCm38 mouse genome[52]. Genes with fewer than 10 read counts in 5 or more
482 samples were removed from all downstream analyses[53].

483

484 ***Single-cell RNA sequencing analysis***

485 Publicly available scRNA-seq data of TIL isolated from control and DIO mice bearing
486 B16-F0 tumors was accessed at GSE245657[8] and processed in R (v4.2.2) using Seurat (v5.0.3)[54].
487 Cells were filtered to include cells with 500-6,500 total reads and with mitochondrial gene
488 expression <10%. 2,491 cells from control mice and 2,373 cells from DIO mice were analyzed.
489 UMAP embeddings were generated using the first 15 principal component analysis components
490 with resolution of 1.3. Canonical correlation analysis was used to integrate control and DIO
491 UMAP embeddings. Redundant clusters were collapsed by Euclidean distance of mean-cluster-
492 wise gene expression using cutree (v4.3.2). Cluster identity was manually assigned from curated
493 gene lists[55]. Any cell with non-zero expression of *GLP1R* was considered *GLP1R* expressing
494 (*GLP1R*+) (~1.5% overall).

495

496 ***Statistical analysis***

497 Statistical analyses were performed using GraphPad Prism (v10.2.2, GraphPad Software
498 Inc., La Jolla, CA) and R (v.4.2.2). Unpaired t-tests compared two groups. One-way ANOVAs
499 with Tukey's post hoc test compared more than two groups. Repeated measures two-way
500 ANOVAs with Šídák's multiple comparisons tests compared two groups across time. Repeated
501 measures one-way ANOVA with Dunnett's multiple comparison test assessed percent viability of
502 tirzepatide-treated cells relative to vehicle-treated cells for the MTT assay. Correlation between
503 tumor burden and body weight was determined by Spearman correlation. Tumor growth over
504 time was assessed using linear regression with false discovery rate (FDR) q-value correction.
505 Differential abundance analysis for high-dimensional flow cytometry analysis was performed
506 using edgeR. Ranked gene expression of *GLP1R*+ cells relative to all other cells from clusters
507 containing at least 1 *GLP1R*+ cell was subject to gene set enrichment analysis[56] using GOBP
508 gene sets[57]. More than 10^7 permutations were performed to ensure stable p values, which were
509 subject to correction using the Benjamini-Hochberg procedure. GSEA of bulk transcriptomic
510 profiling was performed using Hallmark gene sets and 10^3 permutations. Outliers for hormone
511 concentrations and MFIs for phenotypic markers were identified using the ROUT method
512 (Q=5%) and removed. $p<0.05$ was considered statistically significant.

513 **Figure legends**

514 **Figure 1. Tirzepatide (TZP) limits tumor growth in obesity**. **(A)** Study design for chronic TZP
515 treatment in mice bearing subcutaneous MC38 tumors. **(B)** Percent change in body weight over 6
516 weeks with q.o.d. subcutaneous TZP or vehicle injections (n=12/12/12). **(C)** Average calories
517 consumed per mouse for two consecutive 24-hour intervals each week (n=16/16/8). **(D)** MC38
518 tumor volume over time (n=12/12/12). **(E)** Fat mass (n=12/12/12), **(F)** lean mass (n=12/12/12),
519 and **(G)** body composition (n=12/12/12) after 20 days of treatment with TZP or vehicle. **(H)**
520 Fasting blood glucose prior to and following 20 days of TZP (n=12/12/12). Fasting serum
521 concentrations of **(I)** insulin (n=10/10/9), **(J)** glucagon (n=10/10/10), **(K)** leptin (n=9/10/10), **(L)**
522 adiponectin (n=10/10/10), **(M)** adiponectin:leptin (n=10/10/10), and **(N)** IGF-1 (n=10/10/10).

(O) Representative immunohistochemistry staining for Glp1r on pancreas and MC38 tumor sections. Expression levels of *GLP1R* **(P)** and *GIPR* **(Q)** in CCLE RNAseq data. **(R)** MC38 and E0771 cell viability assessed by MTT assay (n=5/group) after 72 h TZP treatment at indicated doses.

Data are represented as mean ± SEM. Statistical significance determined by repeated measures two-way ANOVA with Tukey's multiple comparisons test (B, G), one-way ANOVA with Tukey's multiple comparisons test (C, E-F, I-N), linear regression with FDRq correction (D), paired two-sided Student's t-test (H), or repeated measures one-way ANOVA with Dunnett's multiple comparisons test (R).

Figure 2. Tirzepatide (TZP) restores CD8+ T cell function to limit tumor growth in formerly obese mice. (A) UMAPs of high-dimensional flow cytometry on CD8+ TILs isolated from MC38 tumors of control and DIO mice at 14 days post-transplantation (n=8/8). Staining intensities of selected phenotypic markers driving UMAP projection shown. **(B)** Semi-supervised UMAP clustering of high-dimensional flow cytometry data. **(C)** Differential abundance of TILs from control and DIO mice belonging to identified clusters. **(D)** Relative staining intensities for phenotypic markers across the clusters. **(E)** UMAPs of high-dimensional flow cytometry on CD8+ TILs isolated from MC38 tumors of vehicle- or TZP-treated DIO mice at 14 days post-transplantation (n=8/8). Staining intensities of selected phenotypic markers driving UMAP projection shown. **(F)** Semi-supervised UMAP clustering of high-dimensional flow cytometry data from panel E. **(G)** Differential abundance of TILs from vehicle and TZP-treated DIO mice belonging to identified clusters. **(H)** Relative staining intensities for phenotypic markers across the clusters from panel G. **(I)** CD62L (n=7/8/7), TCF-1 (n=8/8/8), CD39 (n=8/8/8), and PD-1 (n=8/8/8) MFIs from CD8+ TILs. **(J)** MC38 tumor volume over time and **(K)** weights of isotype-treated control, DIO, and TZP mice (n=14/17/18). **(L)** MC38 tumor volume over time and **(M)** weights of αCD8α-treated control, DIO, and TZP mice (n=13/18/17).

Data are represented as mean ± SEM. Statistical significance determined by edgeR differential analysis (C, G), one-way ANOVA with Tukey's multiple comparisons test (I-M), or linear regression with FDRq correction (J, L).

Figure 3. Metabolic dysfunction is essential to achieve an anticancer benefit with tirzepatide (TZP). (A) TZP treatment in lean mice with MC38 subcutaneous tumor transplant study design. **(B)** MC38 tumor volume over time and **(C)** tumor mass (n=15/16). **(D)** Average daily calorie intake per mouse (n=7/7). **(E)** Percent body weight change (n=15/16). **(F)** Fasting blood glucose (n=14/15). **(G)** Blood glucose concentration following intraperitoneal bolus of 1.5 mg/kg D-glucose at indicated time points (n=10/10). Fasting serum concentrations of **(H)** insulin (n=12/10), **(I)** IGF-1 (n=12/11), and **(J)** leptin (n=12/12). **(K)** CD62L (n=8/9) and SlamF6 MFIs from CD8+ TILs. **(L)** CD44 (n=9/9), T-bet (n=10/9), (TOX (n=7/7), and CD27 (n=10/9) MFIs from CD8+ TILs.

Data are represented as mean ± SEM. Statistical significance determined by linear regression with FDRq correction (B) or unpaired two-sided Student's t-test (C-L).

Acknowledgements

The authors acknowledge the Preclinical Research Unit (supported in part by an NCI Center Core Support Grant CA16086 to the Lineberger Comprehensive Cancer Center), the Histology Research Core Facility, and the Genomics and Energy Metabolic Core (supported in part by NIDDK under award number P30DK056350) for their technical assistance in completing this study. This manuscript represents an update of bioRxiv 2023.06.22.546093 (doi: 10.1101/2023.06.22.546093) and bioRxiv 2024.01.20.576484 (doi: 10.1101/2024.01.20.576484).

Author contributions

Conceptualization: E.M.G., M.F.C., G.T.C., B.P.R., V.A.K., E.D.G., J.E.T., M.P., S.D.H.; *Methodology*: E.M.G., M.F.C., G.T.C., B.P.R., V.A.K., E.M.P., E.D.G., J.E.T., M.P., S.D.H.; *Investigation*: E.M.G., M.F.C., G.T.C., B.P.R., A.N.H., T.L.M., V.A.K., A.L.K., E.G.B., K.E.S., J.Z., Y.W., H.M.M., C.E.G., F.C., R.X., C.A.H.; *Formal analysis*: E.M.G., M.F.C., G.T.C., B.P.R., J.E.T., S.D.H.; *Visualization*: E.M.G., M.F.C., G.T.C., B.P.R.; *Writing—original draft:* E.M.G., G.T.C., J.E.T., S.D.H.; *Writing—review & editing:* E.M.G., M.F.C., G.T.C., B.P.R., A.N.H., T.L.M., V.A.K., A.L.K., E.G.B., K.E.S., J.Z., Y.W., H.M.M., C.E.G., F.C., R.X., C.A.H., E.M.P., J.R., E.D.G., J.E.T., M.P., S.D.H.; *Supervision*: E.D.G., J.E.T., M.P., S.D.H.; *Funding acquisition*: E.D.G., J.E.T., M.P., S.D.H.

References

1 WHO. *Obesity and overweight*, <https://www.who.int/news-room/fact-sheets/detail/obesity-and-overweight> (2021).

2 Lauby-Secretan, B. *et al.* Body Fatness and Cancer--Viewpoint of the IARC Working Group. *N Engl J Med* **375**, 794-798 (2016). https://doi.org:10.1056/NEJMsr1606602

3 Ulrich, C. M., Himbert, C., Holowatyj, A. N. & Hursting, S. D. Energy balance and gastrointestinal cancer: risk, interventions, outcomes and mechanisms. *Nat Rev Gastroenterol Hepatol* **15**, 683-698 (2018). https://doi.org:10.1038/s41575-018-0053-2

4 Hopkins, B. D. *et al.* Suppression of insulin feedback enhances the efficacy of PI3K inhibitors. *Nature* **560**, 499-503 (2018). https://doi.org:10.1038/s41586-018-0343-4

5 Lien, E. C. *et al.* Low glycaemic diets alter lipid metabolism to influence tumour growth. *Nature* **599**, 302-307 (2021). https://doi.org:10.1038/s41586-021-04049-2

6 Ringel, A. E. *et al.* Obesity Shapes Metabolism in the Tumor Microenvironment to Suppress Anti-Tumor Immunity. *Cell* **183**, 1848-1866 e1826 (2020). https://doi.org:10.1016/j.cell.2020.11.009

7 Dyck, L. *et al.* Suppressive effects of the obese tumor microenvironment on CD8 T cell infiltration and effector function. *J Exp Med* **219** (2022). https://doi.org:10.1084/jem.20210042

8 Piening, A. *et al.* Obesity-related T cell dysfunction impairs immunosurveillance and increases cancer risk. *Nat Commun* **15**, 2835 (2024). https://doi.org:10.1038/s41467-024-47359-5

9 Zhang, C. *et al.* STAT3 Activation-Induced Fatty Acid Oxidation in CD8(+) T Effector Cells Is Critical for Obesity-Promoted Breast Tumor Growth. *Cell Metab* **31**, 148-161 e145 (2020). https://doi.org:10.1016/j.cmet.2019.10.013

10 van Rijswijk, A. S., van Olst, N., Schats, W., van der Peet, D. L. & van de Laar, A. W. What Is Weight Loss After Bariatric Surgery Expressed in Percentage Total Weight Loss (%TWL)? A Systematic Review. *Obes Surg* **31**, 3833-3847 (2021). https://doi.org:10.1007/s11695-021-05394-x

11 Schauer, D. P. *et al.* Bariatric Surgery and the Risk of Cancer in a Large Multisite Cohort. *Ann Surg* **269**, 95-101 (2019). https://doi.org:10.1097/SLA.0000000000002525

12 English, W. J. *et al.* American Society for Metabolic and Bariatric Surgery 2018 estimate of metabolic and bariatric procedures performed in the United States. *Surg Obes Relat Dis* **16**, 457-463 (2020). https://doi.org:10.1016/j.soard.2019.12.022

13 Hall, K. D. & Kahan, S. Maintenance of Lost Weight and Long-Term Management of Obesity. *Med Clin North Am* **102**, 183-197 (2018). https://doi.org:10.1016/j.mcna.2017.08.012

14 Anderson, A. S. *et al.* Cancer prevention through weight control-where are we in 2020? *Br J Cancer* **124**, 1049-1056 (2021). https://doi.org:10.1038/s41416-020-01154-3

15 Campbell, J. E. *et al.* GIPR/GLP-1R dual agonist therapies for diabetes and weight loss-chemistry, physiology, and clinical applications. *Cell metabolism* **35**, 1519-1529 (2023). https://doi.org:10.1016/j.cmet.2023.07.010

16 Drucker, D. J. The GLP-1 journey: from discovery science to therapeutic impact. *J Clin Invest* **134** (2024). https://doi.org:10.1172/JCI175634

17 Jastreboff, A. M. *et al.* Tirzepatide Once Weekly for the Treatment of Obesity. *N Engl J Med* **387**, 205-216 (2022). https://doi.org:10.1056/NEJMoa2206038

18 Rodriguez, P. J. *et al.* Semaglutide vs Tirzepatide for Weight Loss in Adults With Overweight or Obesity. *JAMA Intern Med* (2024). https://doi.org:10.1001/jamainternmed.2024.2525

19 Rosenstock, J. *et al.* Efficacy and safety of a novel dual GIP and GLP-1 receptor agonist tirzepatide in patients with type 2 diabetes (SURPASS-1): a double-blind, randomised, phase 3 trial. *Lancet (London, England)* **398**, 143-155 (2021). https://doi.org:10.1016/S0140-6736(21)01324-6

20 Packer, M. *et al.* Tirzepatide for Heart Failure with Preserved Ejection Fraction and Obesity. *N Engl J Med* (2024). https://doi.org:10.1056/NEJMoa2410027

21 Jastreboff, A. M. *et al.* Tirzepatide for Obesity Treatment and Diabetes Prevention. *N Engl J Med* **392**, 958-971 (2025). https://doi.org:10.1056/NEJMoa2410819

22 Wang, L., Xu, R., Kaelber, D. C. & Berger, N. A. Glucagon-Like Peptide 1 Receptor Agonists and 13 Obesity-Associated Cancers in Patients With Type 2 Diabetes. *JAMA Netw Open* **7**, e2421305 (2024). https://doi.org:10.1001/jamanetworkopen.2024.21305

23 Pasternak, B. *et al.* Glucagon-like peptide 1 receptor agonist use and risk of thyroid cancer: Scandinavian cohort study. *BMJ (Clinical research ed.)* **385**, e078225 (2024). https://doi.org:10.1136/bmj-2023-078225

24 He, L. *et al.* Association of Glucagon-Like Peptide-1 Receptor Agonist Use With Risk of Gallbladder and Biliary Diseases: A Systematic Review and Meta-analysis of Randomized Clinical Trials. *JAMA Intern Med* **182**, 513-519 (2022). https://doi.org:10.1001/jamainternmed.2022.0338

25 Dankner, R., Murad, H., Agay, N., Olmer, L. & Freedman, L. S. Glucagon-Like Peptide-1 Receptor Agonists and Pancreatic Cancer Risk in Patients With Type 2 Diabetes. *JAMA Netw Open* **7**, e2350408 (2024). https://doi.org:10.1001/jamanetworkopen.2023.50408

26 Wang, L., Berger, N. A., Kaelber, D. C. & Xu, R. Association of GLP-1 Receptor Agonists and Hepatocellular Carcinoma Incidence and Hepatic Decompensation in Patients With Type 2 Diabetes. *Gastroenterology* **167**, 689-703 (2024). https://doi.org:10.1053/j.gastro.2024.04.029

27 Wang, L., Wang, W., Kaelber, D. C., Xu, R. & Berger, N. A. GLP-1 Receptor Agonists and Colorectal Cancer Risk in Drug-Naive Patients With Type 2 Diabetes, With and Without Overweight/Obesity. *JAMA Oncol* **10**, 256-258 (2024). https://doi.org:10.1001/jamaoncol.2023.5573

28 Skriver, C. *et al.* Potential preventive properties of GLP-1 receptor agonists against prostate cancer: a nationwide cohort study. *Diabetologia* **66**, 2007-2016 (2023). https://doi.org:10.1007/s00125-023-05972-x

29 Ibrahim, S. S. *et al.* The effect of GLP-1R agonists on the medical triad of obesity, diabetes, and cancer. *Cancer Metastasis Rev* **43**, 1297-1314 (2024). https://doi.org:10.1007/s10555-024-10192-9

30 Kong, W. *et al.* Tirzepatide as an innovative treatment strategy in a pre-clinical model of obesity-driven endometrial cancer. *Gynecologic Oncology* **191**, 116-123 (2024). https://doi.org:10.1016/j.ygyno.2024.10.004

31 Jeong, B. K. *et al.* A male mouse model for metabolic dysfunction-associated steatotic liver disease and hepatocellular carcinoma. *Nat Commun* **15**, 6506 (2024). https://doi.org:10.1038/s41467-024-50660-y

32 Marathe, S. J. *et al.* Incretin triple agonist retatrutide (LY3437943) alleviates obesity-associated cancer progression. *npj Metabolic Health and Disease* **3**, 10 (2025). https://doi.org:10.1038/s44324-025-00054-5

33 Coskun, T. *et al.* LY3298176, a novel dual GIP and GLP-1 receptor agonist for the treatment of type 2 diabetes mellitus: From discovery to clinical proof of concept. *Mol Metab* **18**, 3-14 (2018). https://doi.org:10.1016/j.molmet.2018.09.009

34 Samms, R. J. *et al.* GIPR agonism mediates weight-independent insulin sensitization by tirzepatide in obese mice. *J Clin Invest* **131** (2021). https://doi.org:10.1172/JCI146353

35 Ast, J., Broichhagen, J. & Hodson, D. J. Reagents and models for detecting endogenous GLP1R and GIPR. *EBioMedicine* **74**, 103739 (2021). https://doi.org:10.1016/j.ebiom.2021.103739

36 Barretina, J. *et al.* The Cancer Cell Line Encyclopedia enables predictive modelling of anticancer drug sensitivity. *Nature* **483**, 603-607 (2012). https://doi.org:10.1038/nature11003

37 Costa, S. S. F. *et al.* Robust inference of expression state in bulk and single-cell RNA-Seq using curated intergenic regions. *bioRxiv*, 2022.2003.2031.486555 (2022). https://doi.org:10.1101/2022.03.31.486555

38 El, K. *et al.* The incretin co-agonist tirzepatide requires GIPR for hormone secretion from human islets. *Nat Metab* **5**, 945-954 (2023). https://doi.org:10.1038/s42255-023-00811-0

39 Ben Nasr, M. *et al.* Glucagon-like peptide 1 receptor is a T cell-negative costimulatory molecule. *Cell metabolism* **36**, 1302-1319 e1312 (2024). https://doi.org:10.1016/j.cmet.2024.05.001

40 Wong, C. K. *et al.* Central glucagon-like peptide 1 receptor activation inhibits Toll-like receptor agonist-induced inflammation. *Cell Metab* **36**, 130-143 e135 (2024). https://doi.org:10.1016/j.cmet.2023.11.009

41 Wong, C. K. *et al.* Divergent roles for the gut intraepithelial lymphocyte GLP-1R in control of metabolism, microbiota, and T cell-induced inflammation. *Cell metabolism* **34**, 1514-1531 e1517 (2022). https://doi.org:10.1016/j.cmet.2022.08.003

42 Wang, Z. *et al.* Paradoxical effects of obesity on T cell function during tumor progression and PD-1 checkpoint blockade. *Nat Med* **25**, 141-151 (2019). https://doi.org:10.1038/s41591-018-0221-5

43 Bader, J. E. *et al.* Obesity induces PD-1 on macrophages to suppress anti-tumour immunity. *Nature* **630**, 968-975 (2024). https://doi.org:10.1038/s41586-024-07529-3

44 Bowers, L. W. *et al.* Reversing the genomic, epigenetic and triple negative breast cancer-enhancing effects of obesity. *Cancer Prev Res (Phila)* (2022). https://doi.org:10.1158/1940-6207.CAPR-22-0113

45 Camp, K. K. *et al.* Calorie restriction outperforms bariatric surgery in a murine model of obesity and triple-negative breast cancer. *JCI Insight* **8** (2023). https://doi.org:10.1172/jci.insight.172868

46 Zhao, Z. *et al.* Intermittent energy restriction inhibits tumor growth and enhances paclitaxel response in a transgenic mouse model of endometrial cancer. *Gynecol Oncol* **186**, 126-136 (2024). https://doi.org:10.1016/j.ygyno.2024.04.012

47 Itoh, A. *et al.* GLP-1 receptor agonist, liraglutide, ameliorates hepatosteatosis induced by anti-CD3 antibody in female mice. *J Diabetes Complications* **31**, 1370-1375 (2017). https://doi.org:10.1016/j.jdiacomp.2017.05.013

48 Moschovaki Filippidou, F. *et al.* Glucagon-Like Peptide-1 Receptor Agonism Improves Nephrotoxic Serum Nephritis by Inhibiting T-Cell Proliferation. *Am J Pathol* **190**, 400-411 (2020). https://doi.org:10.1016/j.ajpath.2019.10.008

49 Giles, E. D. & Wellberg, E. A. Preclinical Models to Study Obesity and Breast Cancer in Females: Considerations, Caveats, and Tools. *J Mammary Gland Biol Neoplasia* **25**, 237-253 (2020). https://doi.org:10.1007/s10911-020-09463-2

50 Euhus, D. M., Hudd, C., LaRegina, M. C. & Johnson, F. E. Tumor measurement in the nude mouse. *J Surg Oncol* **31**, 229-234 (1986). https://doi.org:10.1002/jso.2930310402

51 Bolger, A. M., Lohse, M. & Usadel, B. Trimmomatic: a flexible trimmer for Illumina sequence data. *Bioinformatics* **30**, 2114-2120 (2014). https://doi.org:10.1093/bioinformatics/btu170

52 Dobin, A. *et al.* STAR: ultrafast universal RNA-seq aligner. *Bioinformatics* **29**, 15-21 (2013). https://doi.org:10.1093/bioinformatics/bts635

53 Love, M. I., Huber, W. & Anders, S. Moderated estimation of fold change and dispersion for RNA-seq data with DESeq2. *Genome Biol* **15**, 550 (2014). https://doi.org:10.1186/s13059-014-0550-8

54 Hao, Y. *et al.* Dictionary learning for integrative, multimodal and scalable single-cell analysis. *Nature biotechnology* **42**, 293-304 (2024). https://doi.org:10.1038/s41587-023-01767-y

55 Daniel, B. *et al.* Divergent clonal differentiation trajectories of T cell exhaustion. *Nat Immunol* **23**, 1614-1627 (2022). https://doi.org:10.1038/s41590-022-01337-5

56 Subramanian, A. *et al.* Gene set enrichment analysis: a knowledge-based approach for interpreting genome-wide expression profiles. *Proc Natl Acad Sci U S A* **102**, 15545-15550 (2005). https://doi.org:10.1073/pnas.0506580102

57 Gene Ontology, C. *et al.* The Gene Ontology knowledgebase in 2023. *Genetics* **224** (2023). https://doi.org:10.1093/genetics/iyad031

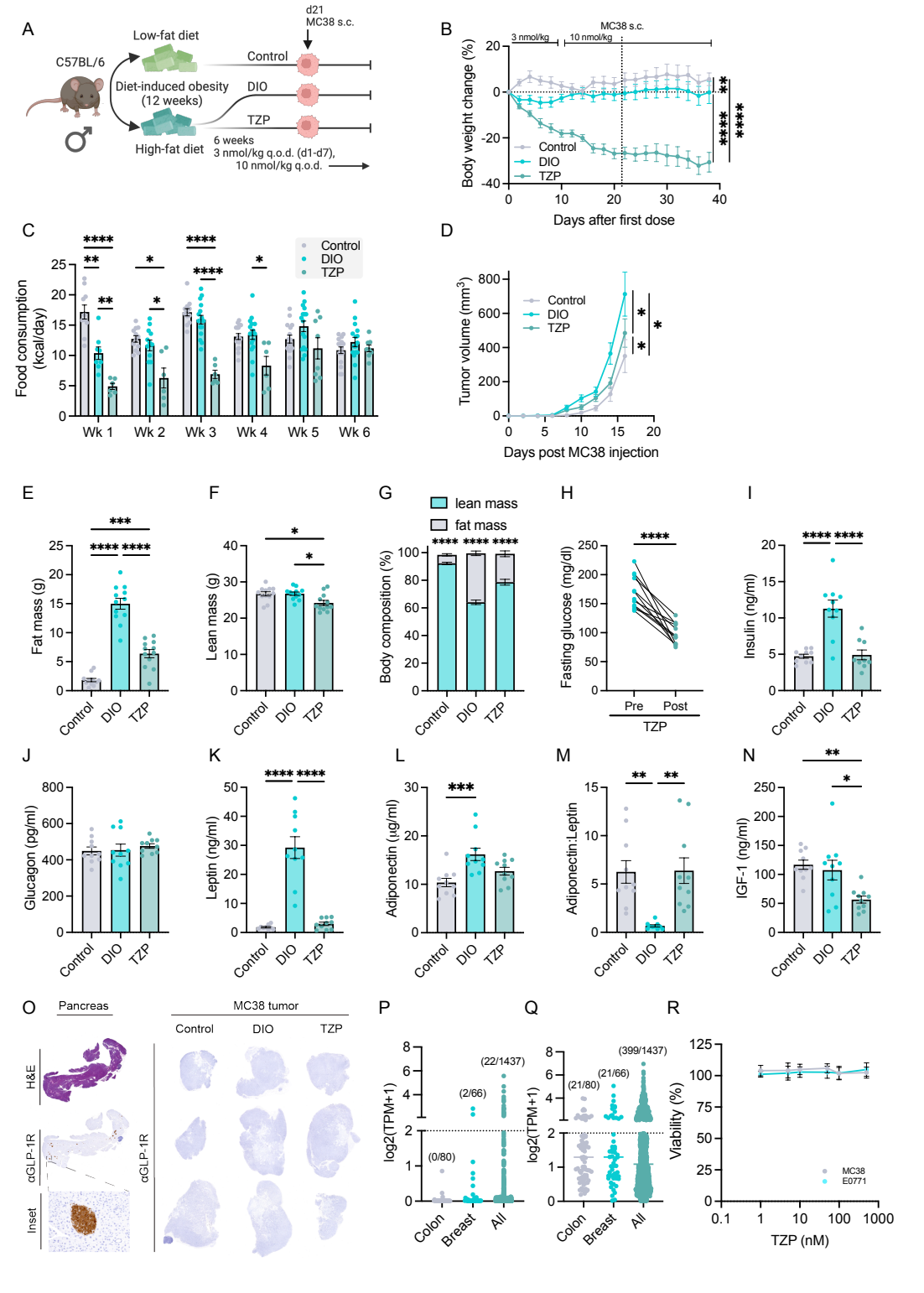
A
C57BL/6
Low-fat diet
Diet-induced obesity (12 weeks)
High-fat diet
d21 MC38 s.c.
Control
DIO
TZP
6 weeks
3 nmol/kg q.o.d. (d1-d7),
10 nmol/kg q.o.d.
B
MC38 s.c.
3 nmol/kg
10 nmol/kg
Body weight change (%)
Days after first dose
C
Food consumption (kcal/day)
Wk 1
Wk 2
Wk 3
Wk 4
Wk 5
Wk 6
D
Tumor volume (mm³)
Days post MC38 injection
E
Fat mass (g)
F
Lean mass (g)
G
lean mass
fat mass
Body composition (%)
H
Fasting glucose (mg/dl)
Pre
Post
TZP
I
Insulin (ng/ml)
J
Glucagon (pg/ml)
K
Leptin (ng/ml)
L
Adiponectin (µg/ml)
M
Adiponectin:Leptin
N
IGF-1 (ng/ml)
O
Pancreas
MC38 tumor
H&E
αGLP-1R
Inset
P
log2(TPM+1)
(22/1437)
(2/66)
(0/80)
Colon
Breast
All
Q
(399/1437)
(21/66)
(21/80)
R
Viability (%)
MC38
E0771
TZP (nM)

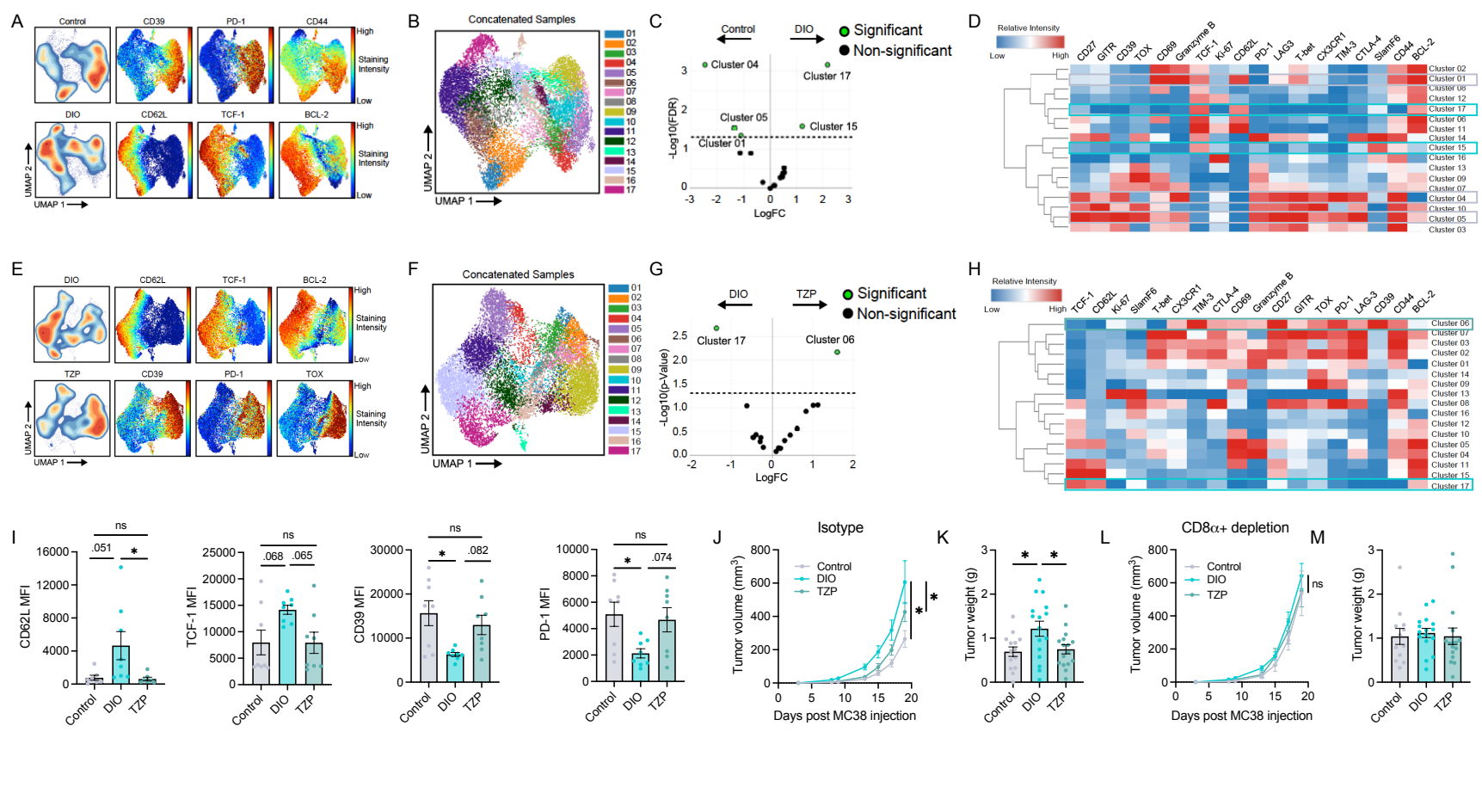
A
Control
CD39
PD-1
CD44
DIO
CD62L
TCF-1
BCL-2
High
Staining Intensity
Low
UMAP 2
UMAP 1
B
Concatenated Samples
01
02
03
04
05
06
07
08
09
10
11
12
13
14
15
16
17
C
Control
DIO
Significant
Non-significant
Cluster 04
Cluster 17
Cluster 05
Cluster 15
Cluster 01
-Log10(FDR)
LogFC
D
Relative Intensity
Low
High
CD27
GITR
CD39
TOX
CD69
Granzyme B
TCF-1
Ki-67
CD62L
PD-1
LAG3
T-bet
CX3CR1
TIM-3
CTLA-4
SlamF6
CD44
BCL-2
Cluster 02
Cluster 01
Cluster 08
Cluster 12
Cluster 17
Cluster 06
Cluster 11
Cluster 14
Cluster 15
Cluster 16
Cluster 13
Cluster 09
Cluster 07
Cluster 04
Cluster 10
Cluster 05
Cluster 03
E
DIO
CD62L
TCF-1
BCL-2
TZP
CD39
PD-1
TOX
High
Staining Intensity
Low
UMAP 2
UMAP 1
F
Concatenated Samples
01
02
03
04
05
06
07
08
09
10
11
12
13
14
15
16
17
G
DIO
TZP
Significant
Non-significant
Cluster 17
Cluster 06
-Log10(p-Value)
LogFC
H
Relative Intensity
Low
High
TCF-1
CD62L
Ki-67
SlamF6
T-bet
CX3CR1
TIM-3
CTLA-4
CD69
Granzyme B
CD27
GITR
TOX
PD-1
LAG3
CD39
CD44
BCL-2
Cluster 06
Cluster 07
Cluster 03
Cluster 02
Cluster 01
Cluster 14
Cluster 09
Cluster 13
Cluster 08
Cluster 16
Cluster 12
Cluster 10
Cluster 05
Cluster 04
Cluster 11
Cluster 15
Cluster 17
I
ns
.051
*
CD62L MFI
.068
.065
TCF-1 MFI
.082
CD39 MFI
.074
PD-1 MFI
Control
DIO
TZP
J
Isotype
Control
DIO
TZP
Tumor volume (mm³)
Days post MC38 injection
K
Tumor weight (g)
L
CD8α+ depletion
ns
M

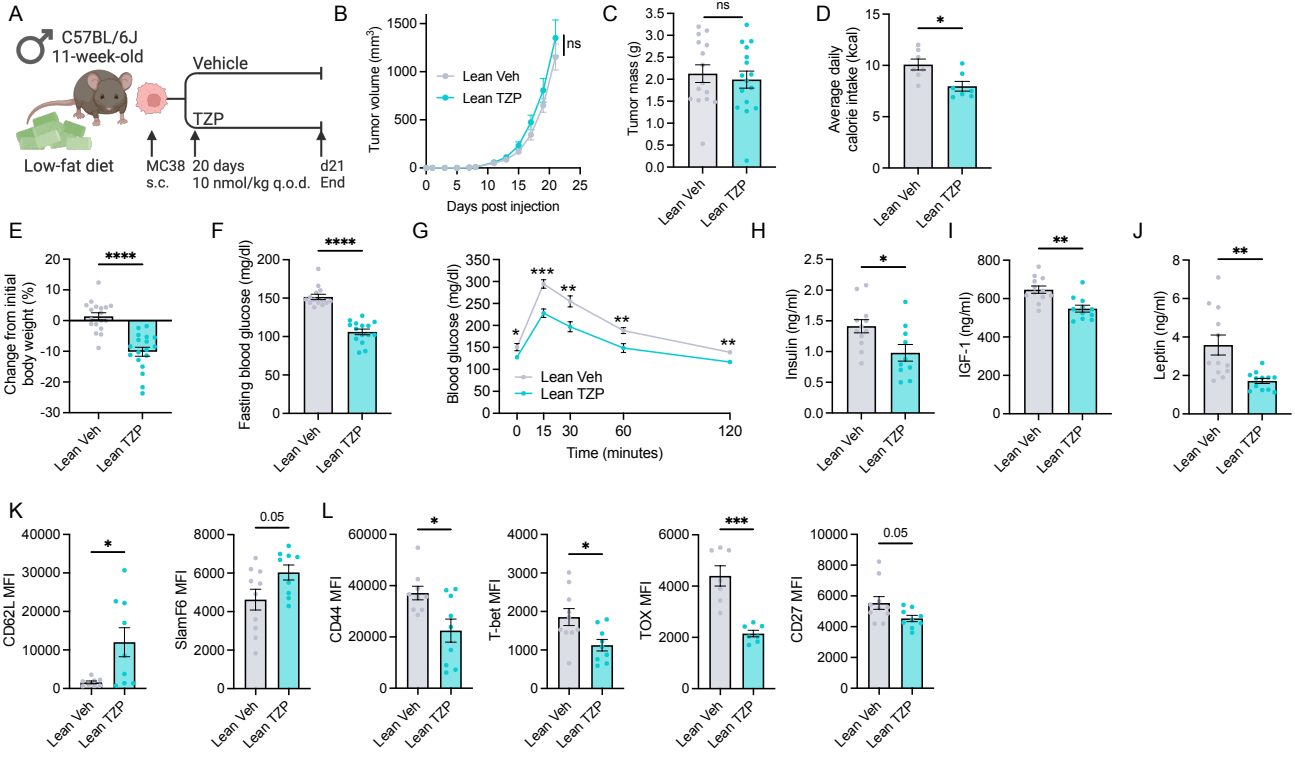
A
♂ C57BL/6J
11-week-old
Vehicle
TZP
Low-fat diet
MC38
s.c.
20 days
10 nmol/kg q.o.d.
d21
End
B
Tumor volume (mm³)
Lean Veh
Lean TZP
ns
Days post injection
C
Tumor mass (g)
ns
D
Average daily calorie intake (kcal)
*
E
Change from initial body weight (%)
****
F
Fasting blood glucose (mg/dl)
****
G
Blood glucose (mg/dl)
Time (minutes)
H
Insulin (ng/ml)
*
I
IGF-1 (ng/ml)
**
J
Leptin (ng/ml)
**
K
CD62L MFI
*
SlamF6 MFI
0.05
L
CD44 MFI
*
T-bet MFI
*
TOX MFI
***
CD27 MFI
0.05